



Ultrafast ionic diffusion of debossed carbon nanocomposites for lithium storage



Geon-Hyoung An ^a, Young-Geun Lee ^b, Hyo-Jin Ahn ^{a,b,*}

^a Program of Materials Science & Engineering, Convergence Institute of Biomedical Engineering and Biomaterials, Seoul National University of Science and Technology, Seoul 139-743, South Korea

^b Department of Materials Science and Engineering, Seoul National University of Science and Technology, Seoul 139-743, South Korea

ARTICLE INFO

Article history:

Received 23 April 2018

Received in revised form

6 June 2018

Accepted 7 June 2018

ABSTRACT

Owing to their superb mechanical durability resulting from the dramatic volume changes of the Sn nanoparticles and high electrical conductivity, carbon and tin (Sn) nanocomposites have received an increasing attention in view of their application as anode materials for lithium ion batteries (LIBs). However, due to the poor ionic diffusion capability for Li ions during the cycling, the low ultrafast performance for energy storage remains rather limited. In the present study, aiming to improve the ionic diffusion capability for Li ions, we suggest a novel design of the debossed structure of carbon and Sn nanocomposites by electrospinning, carbonization, and the debossing process. The electrode based on the debossed structure exhibits a noticeable cycling stability and high discharge capacity (677 mA h g⁻¹ after 100 cycles at 100 mA g⁻¹), an excellent rate capability (482 mA h g⁻¹ at 2000 mA g⁻¹), and an outstanding ultrafast cycling stability (275 mA h g⁻¹ after 500 cycles at 2000 mA g⁻¹). Therefore, this novel design of the debossed structure based on carbon and Sn nanocomposites offers attractive effects, such as the effective accommodation of dramatic volume changes for the Sn nanoparticles, as well as an improved ionic diffusion performance of Li ions.

© 2018 Elsevier B.V. All rights reserved.

1. Introduction

The rapid consumption of fossil fuels and the growing anxiety regarding environmental contamination have stimulated the search for renewable and clean energy sources and the development of advanced energy storage technologies, which are among the most significant issues worldwide. Furthermore, the fast-growing industry of electric transportations and portable electronics has caused a strong need for the development of lithium-ion batteries (LIBs) that would be characterized by a high energy density, long lifespan, and environmental friendliness [1–5].

In the near future, the target of LIBs will focus on the use of electric means of transportation, such as electric vehicles and electric bikes. However, due to the sluggish kinetics of Li ions during the cycling, the rate capability of LIBs remains to be a big challenge [6–9]. For example, the Tesla Model 3 using the commercial LIBs need a long charging time: 20–30 h at home or

5–6 h at a home charging point. The enhancement of LIBs with the ultrafast capability (called ultrafast LIBs) is directly related to reducing the charging time. However, due to the rapid ionic diffusion in an anode electrode during the cycling, which leads to a low capacity at high current densities, the ultrafast technologies of LIBs remain to be a challenge.

Until now, much effort has been invested to find the way to the capacity and cycling stability of anode materials consisting of the high capacity nanomaterials (e.g. metal or metal oxide) and carbon composites [10–15]. These composite materials could effectively accommodate the dramatic volume changes of metal or metal oxide and increase the electrical conductivity, leading thus to an improved electrochemical performance. However, the challenges faced by this concept include the poor ultrafast capability; accordingly, the anode material needs a new way to enhance the excellent ionic diffusion capability.

In this context, the present study proposes a novel nano-architecture of the debossed carbon nanofiber with the tin (Sn) nanoparticles (DCNF/Sn), where Sn was used as a typical high-capacity metal (992 mA h g⁻¹) [16–18]. The carbon nanofiber (referred to as CNF) was used as a matrix for the Sn nanoparticles to

* Corresponding author. Department of Materials Science and Engineering, Seoul National University of Science and Technology, Seoul 139-743, South Korea.

E-mail address: hjahn@seoultech.ac.kr (H.-J. Ahn).

accommodate the dramatic volume changes. Furthermore, the key technology of this concept was the debossed structure to obtain an excellent ionic diffusion capability, which is an opener to acquire the outstanding ultrafast capability at high current densities. For comparison, the CNF with the Sn nanoparticles (referred to as CNF/Sn) without the debossed structure were used.

2. Results and discussion

Fig. 1 illustrates the synthetic process of DCNF/Sn. First, the as-nanofiber consisting of polyacrylonitrile (PAN, $M_w = 150,000$), tin(II) chloride dihydrate ($\text{SnCl}_2 \cdot 2\text{H}_2\text{O}$), and the Si nanoparticles (50–80 nm) was prepared by electrospinning (see **Fig. 1a**). After carbonization in the nitrogen atmosphere, the carbon nanofiber with embedded the Si and Sn nanoparticles was fabricated (see **Fig. 1b**). Finally, the debossing process by the hydrofluoric acid was employed to eliminate the Si nanoparticles. Therefore, we successfully synthesized the novel nanoarchitecture of DCNF/Sn by electrospinning, carbonization, and the debossing process (see **Fig. 1c**).

Fig. 2 shows indicates low-resolution (**Fig. 2a–c**) and high-resolution (**Fig. 2d–f**) scanning electron microscopy (SEM) images of CNF, CNF/Sn, and DCNF/Sn. CNF (see **Fig. 2a** and d) has the flat surface, which can effectively accommodate the dramatic volume changes of metal or metal oxide, leading to an improved electrochemical performance. CNF/Sn (**Fig. 2b** and e) also displays the flat surface without any nanoparticles on the surface, intimating the almost embedded Sn nanoparticles in CNF. As can be seen in **Fig. 2c** and f, DCNF/Sn had the craters on the surface due to the elimination of the Si nanoparticles by the debossing process; therefore, it can be expected that improved ionic diffusion capability will significantly enhance the ultrafast performance of LIBs.

The transmission electron microscopy (TEM, Korea Basic Science Institute, Gwangju Center) analysis was performed to further identify the nanostructural properties using low-resolution (**Fig. 3a–c**) and high-resolution (**Fig. 3d–f**) images of CNF, CNF/Sn, and DCNF/Sn. The as-spun nanofiber showed well-dispersed Si nanoparticles in the PAN nanofiber, which could develop the debossed structure of DCNF/Sn (see **Fig. S1** in Supporting

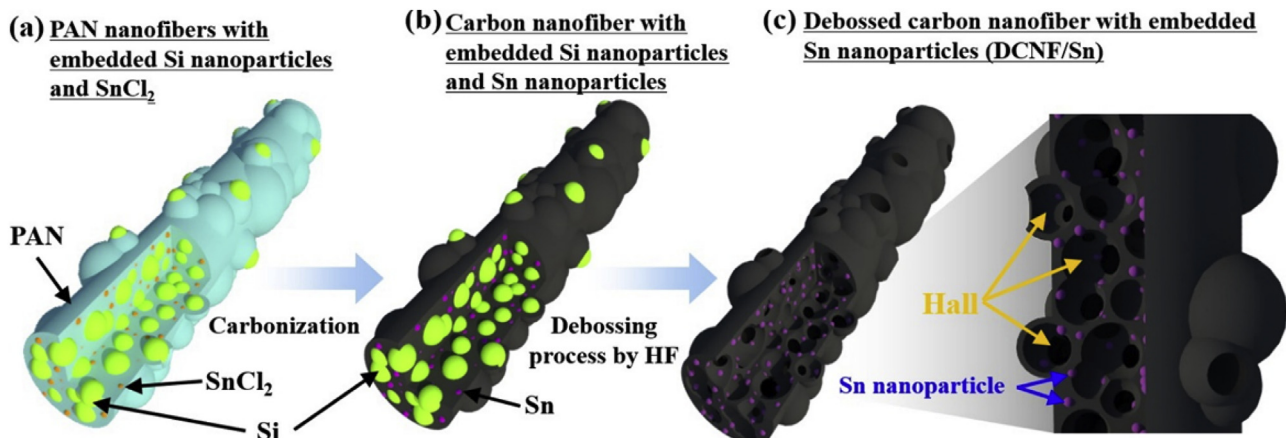


Fig. 1. Schematic illustration of the fabrication process for (a) the PAN nanofibers with the embedded Si nanoparticles and SnCl_2 ; (b) carbon nanofiber with the embedded Si nanoparticles and Sn nanoparticles; and (c) debossed carbon nanofiber with embedded Sn nanoparticles (DCNF/Sn).

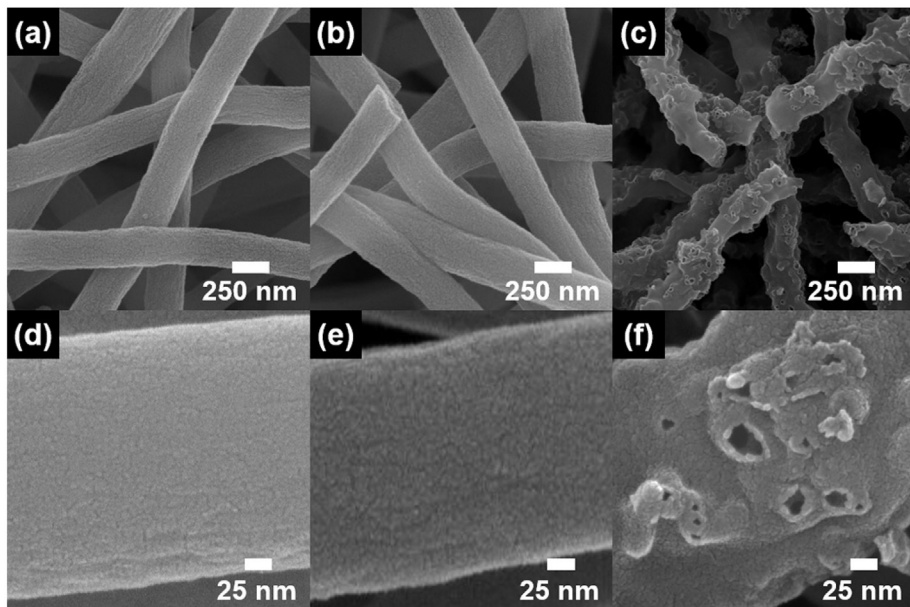


Fig. 2. (a–c) Low-resolution and (d–f) high-resolution SEM images of CNF, CNF/Sn, and DCNF/Sn.

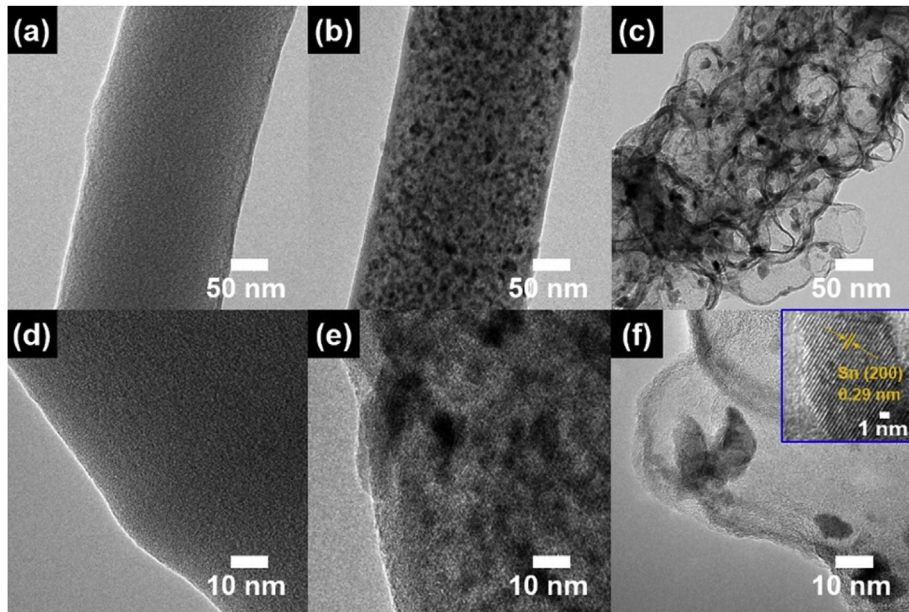


Fig. 3. (a–c) Low-resolution and (d–f) high-resolution TEM images of CNF, CNF/Sn, and DCNF/Sn.

Information). CNF (Fig. 3a and d) showed a uniform contrast, signifying only one phase of carbon. The Sn nanoparticles (in size of 7–16 nm) of CNF/Sn (Fig. 3b and e) were completely embedded into the carbon matrix. This structure is useful in terms of improving the high capacity and cycling stability of LIBs by the accommodation of dramatic volume changes for the Sn nanoparticles. However, at the high current densities, the conventional nanocomposites consisting of carbon and the Sn nanoparticles showed a poor ultrafast performance due to the deficient ionic diffusion capability [15–21]. Furthermore, DCNF/Sn (Fig. 3c and f) exhibited the debossed structure consisting of halls (40–90 nm in size) as well as the Sn

nanostructures embedded into the carbon matrix. In addition, the Sn nanoparticle of DCNF/Sn showed the lattice spacing of 0.29 nm, corresponding to the (200) plane of Sn [7,22,23]. Therefore, the novel debossed structure of DCNF/Sn may result in well-dispersed Sn nanoparticles in the carbon matrix, which can directly improve the ionic diffusion capability and the efficient transfer way for electrons during cycling.

Fig. 4a shows the X-ray diffractometry (XRD) data of CNF, CNF/Sn, and DCNF/Sn conducted to inspect the crystal properties. All nanofibers exhibited broad peaks around 25° , which corresponds to the (002) plane of graphite [24–26]. The diffraction data of pure

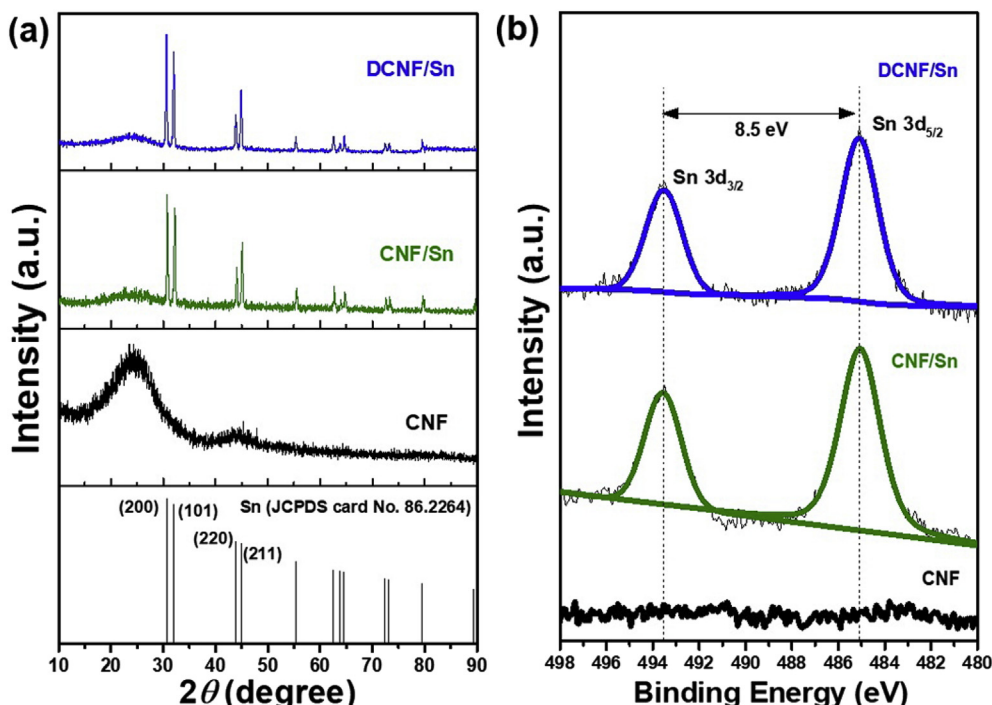


Fig. 4. (a) The XRD patterns and (b) XPS spectra of Sn 3d for CNF, CNF/Sn, and DCNF/Sn.

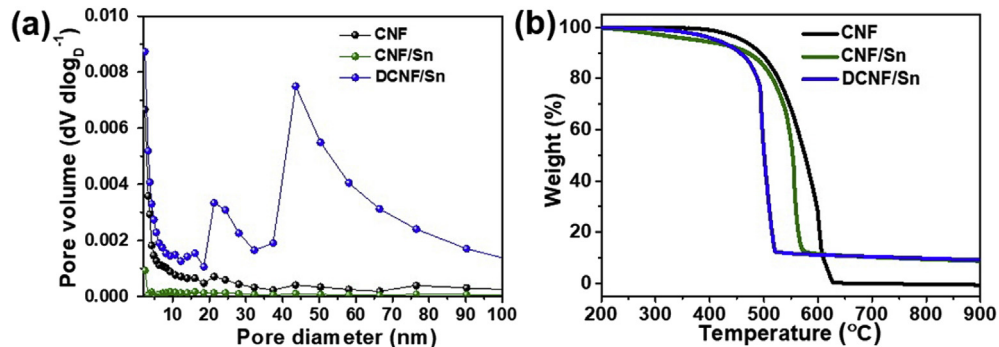


Fig. 5. (a) The BJH pore size distributions and (b) the TGA curves from 200 to 900 °C at the heating rate of 10 °C min⁻¹ in air of CNF, CNF/Sn, and DCNF/Sn.

Sn is presented for comparison. The main peaks of CNF/Sn and DCNF/Sn were observed at 30.6°, 32.0°, 43.9°, and 44.9°, corresponding to the (200), (101), (220), and (211) planes of Sn. Therefore, the XRD outcomes show that the debossing process was not a crystallinity transformation of Sn. To further explore the chemical bonding states on the surface, X-ray photoelectron spectroscopy (XPS) was performed (see Fig. 4b). The Sn 3d spectrum of CNF is not visible. On the other hand, the Sn 3d spectra of CNF/Sn and DCNF/Sn can be divided into two peaks located at 485.0 and 493.5 eV with the spin energy separation of 8.5 eV, which are identified to 3d_{3/2} and 3d_{5/2} photoelectrons of metallic Sn, respectively [7].

To inspect the porous structure of CNF, CNF/Sn, and DCNF/Sn, N₂ adsorption/desorption isotherms were executed using the Barrett–Joyner–Halenda (BJH) analysis (see Fig. 5a). Consistently with the SEM and TEM results, the CNF and CNF/Sn presented a low mesopore distribution from 2 to 100 nm, implying the micropores structure (>2 nm) with a poor ionic diffusion capability at high current densities during cycling. At the same time, DCNF/Sn showed a high mesopore distribution from 40 to 90 nm. Therefore, the development of the debossed structure for DCNF/Sn was successfully prepared to enhance the ionic diffusion capability. To

further investigate the contents of CNF, CNF/Sn, and DCNF/Sn, the thermogravimetric analysis (TGA) measurement was conducted in the heating rate of 10 °C min⁻¹ in the air from 200 °C to 900 °C (see Fig. 5b). CNF showed the weight loss of 100%, signifying there being only one phase of carbon without impurities. Moreover, the weight loss of both CNF/Sn and DCNF/Sn amounted to 89%, implying the presence of the Sn nanoparticles. These results confirm the debossed structural effect for the ultrafast performance of LIBs. The electrochemical behaviors were analyzed with the Li metal as the counter electrode. Electrochemical impedance spectroscopy (EIS) was performed to study the effect of the debossed structure on the electrochemical performance in the anode materials.

Fig. 6a shows the Nyquist plots in the frequency range of 10⁵–10⁻² Hz. The semicircle in the high-frequency refers to the charge transfer resistance (R_{ct}), and it can be seen that, compared to the CNF electrode, R_{ct} of CNF/Sn and DCNF/Sn electrode is small. The reduced values of R_{ct} demonstrate the improved charge transfer kinetics from the embedded Sn nanoparticles in the carbon matrix. In addition, in the low-frequency, the slope means the diffusion performance of Li ions (called Warburg impedance). The straight sloping line of DCNF/Sn electrode indicates the lowest Warburg

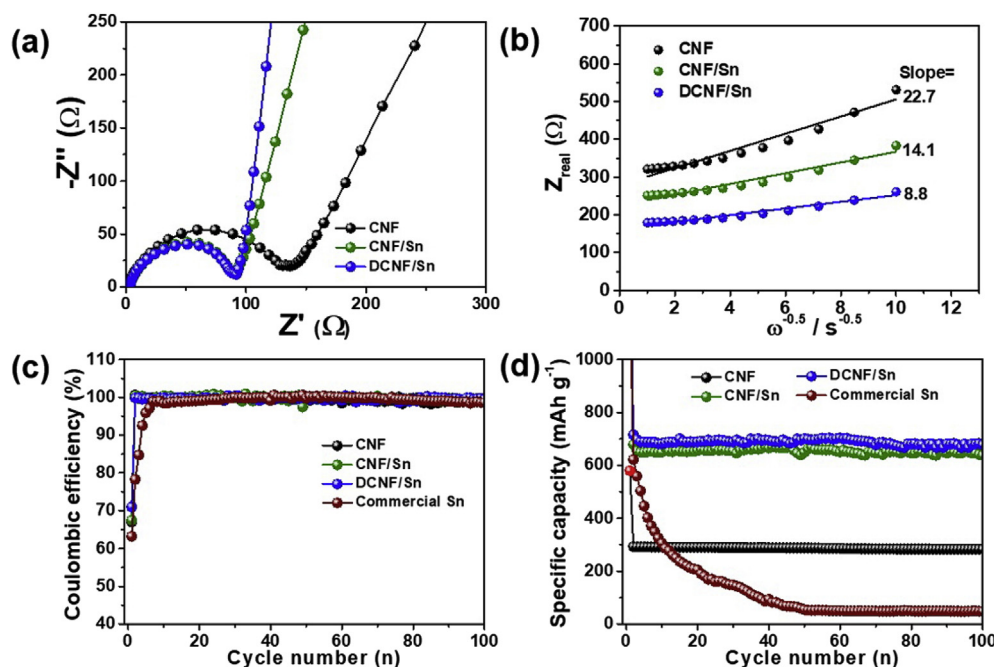


Fig. 6. (a) Nyquist plots in the frequency range of 10⁵–10⁻² Hz; (b) The relationship between $\omega^{-1/2}$ and Z_{real} ; (c) Coulombic efficiency; (d) cycling stability of the CNF, CNF/Sn, DCNF/Sn, and commercial Sn electrodes at the current density of 100 mA g⁻¹ over 100 cycles.

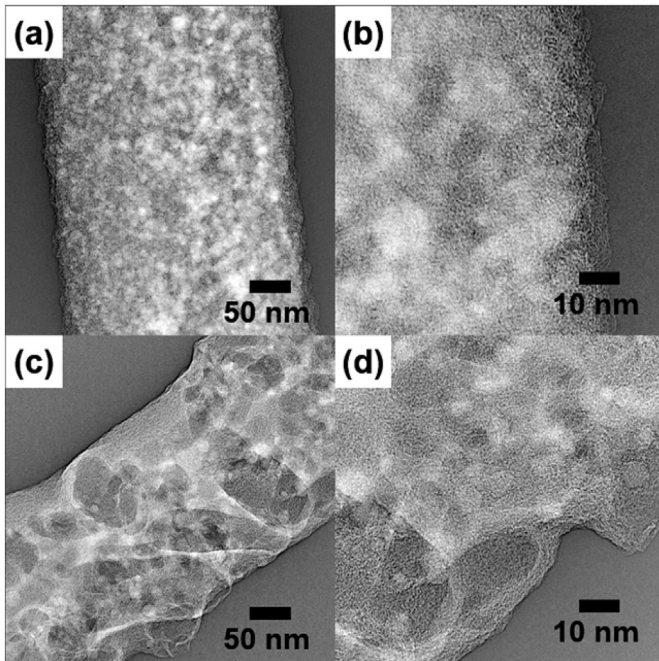


Fig. 7. TEM images of (a and b) CNF/Sn and (c and d) DCNF/Sn at a current density of 100 mA g^{-1} after 100 cycles.

impedance that results from a shorter diffusion pathway of Li ions as compared to other electrodes. Furthermore, the Warburg impedance coefficients (σ_w) could be evaluated using sloping lines in the low frequency as Warburg impedance by the square root of the frequency ($\omega^{-1/2}$) and Z_{real} (see Eqs. (1) and (2)) [3,27].

$$Z_{\text{real}} = R_e + R_{\text{ct}} + \sigma_w \omega^{-1/2} \quad (1)$$

$$D = R^2 T^2 / 2 A^2 n^4 F^4 C^2 \sigma_w^2 \quad (2)$$

where D is a Li diffusion coefficient, R is a constant of gas, T is temperature, A is an electrode area, n is a number of electron/molecule, F is Faraday's constant, and C is the molar concentration of Li ions. Fig. 6b shows the relationship between $\omega^{-1/2}$ and Z_{real} . σ_w value of CNF, CNF/Sn, and DCNF/Sn electrodes amounted to 22.7, 14.1, and $8.8 \Omega \text{ cm}^2 \text{ s}^{-1/2}$, respectively. The diffusion capability of Li ions was obtained by σ_w value. The Li diffusion coefficient of the CNF, CNF/Sn, and DCNF/Sn electrodes was 6.6×10^{-13} , 1.7×10^{-12} , and $4.3 \times 10^{-12} \text{ cm}^2 \text{ s}^{-1}$, respectively. These consequences confirm an improvement of ionic diffusion performance for Li ions based on the debossed structure of the DCNF/Sn electrode. To identify the energy storage performance of the CNF, CNF/Sn, and DCNF/Sn electrodes, the charging and discharging tests were performed between 0.05 and 3.00 V over 100 cycles at the current rate of 100 mA g^{-1} (see Fig. 6c–d). Moreover, the commercial Sn nanoparticles were prepared for comparison. The Coulombic efficiency at the first cycles of the CNF, CNF/Sn, DCNF/Sn, and commercial Sn electrodes amounted to 67.0, 67.5, 71.0, and 63.2%, respectively (see Fig. 6c). The initial irreversible reactions can be ascribed to the development of the solid-electrolyte interphase layers on the electrode surface due to the reductive disintegration of the electrolyte [3,5,7]. However, compared to other electrodes, the DCNF/Sn electrode showed a high initial Coulombic efficiency, which signifies the favourable effect of the debossed structure. In addition, the Coulombic efficiency of all electrodes reached 100% after 7 cycles, which means that the prepared materials for electrode has the excellent reversible activity. Fig. 6d shows the cycling stability with the discharge capacities of the CNF, CNF/Sn, DCNF/Sn, and commercial Sn electrodes over 100 cycles at the current density of 100 mA g^{-1} . The CNF electrode exhibited the outstanding cycling stability with the discharge capacity of 283 mAh g^{-1} after 100 cycles, implying that it is an excellent candidate for the matrix to

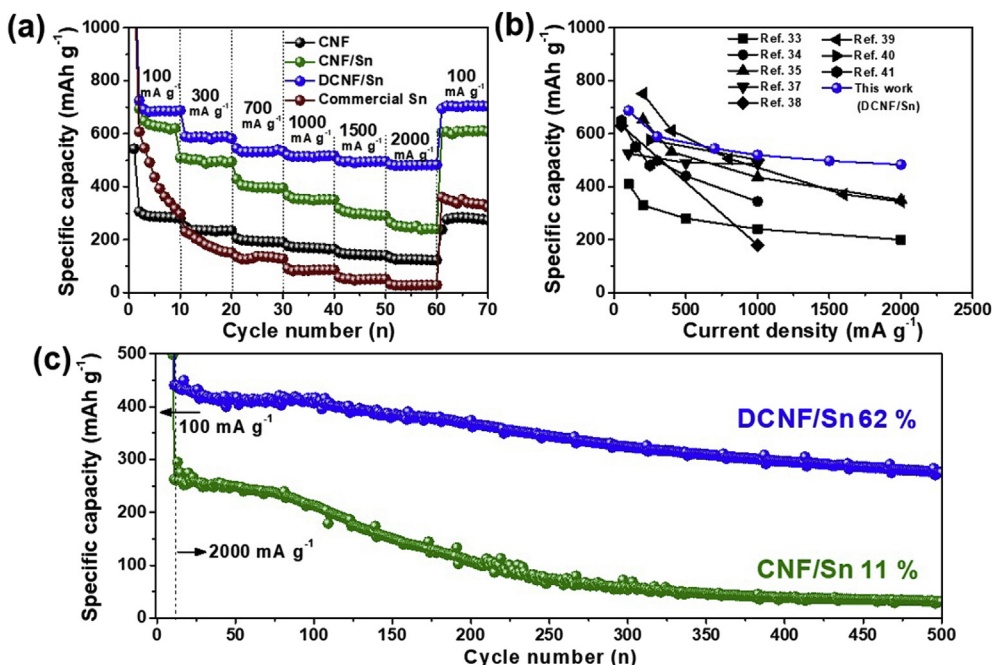


Fig. 8. (a) Rate capability of the CNF, CNF/Sn, DCNF/Sn, and commercial Sn electrodes at different current densities ranging from 100 to 2000 mA g^{-1} ; (b) Comparison of high-rate performance with the previously reported electrodes using carbon and Sn nanocomposites in LIBs; (c) Ultrafast cycling stability at the current density of 2000 mA g^{-1} over 500 cycles.

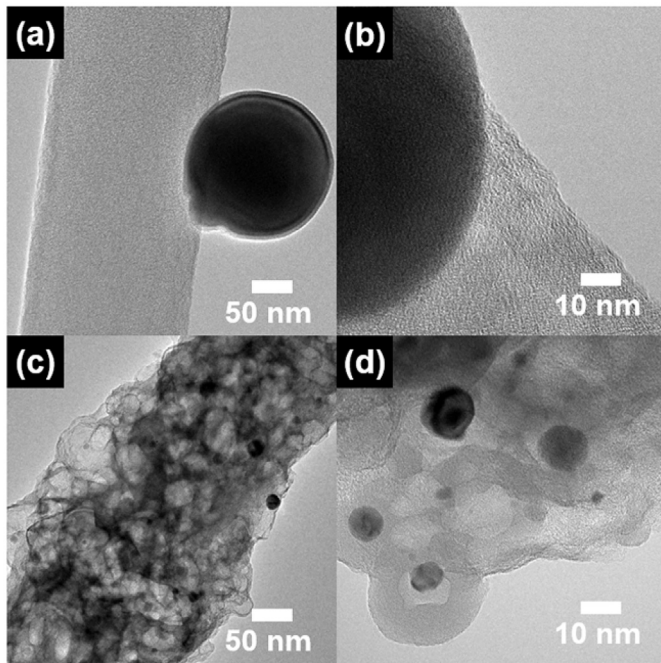


Fig. 9. TEM images of (a and b) CNF/Sn and (c and d) DCNF/Sn at a current density of 2000 mA g^{-1} after 500 cycles.

accommodate of dramatic volume changes. On the other hand, the commercial Sn electrode showed a poor cycling stability with the discharge specific capacity of 49 mAh g^{-1} after 100 cycles, suggesting a necessity of carbon and Sn nanocomposites to improve the electrochemical performance. Obviously, the CNF/Sn and DCNF/Sn electrodes had an outstanding cycling stability of with the discharge specific capacity of 638 mAh g^{-1} and 677 mAh g^{-1} after 100 cycles, indicating that the introduction of porous carbon could provide the numerable electrochemical reaction sites with the improved kinetic properties and accommodation of dramatic volume changes for the Sn nanoparticles. Especially, the DCNF/Sn electrode held a higher discharge specific capacity than the previously reported electrodes using carbon and Sn nanocomposites (see Table S1) [28–37].

In addition, the structure of CNF/Sn (see Fig. 7a and b) and DCNF/Sn (see Fig. 7c and d) remained constant with regard to the initial structure after 100 cycles. Nevertheless, the Sn nanoparticles

showed the no significant lattice fringe, which means the change to amorphous structure after cycling [2,4,5].

The rapid expansion of application areas of LIBs has stimulated considering rate and ultrafast performance, which are the most significant issues in anode materials of LIBs. Fig. 8a shows the outcomes of the rate capability test from 100 mA g^{-1} to 2000 mA g^{-1} . It is clear that the discharge specific capacities of all electrodes decrease according to the raise of current density because of the reduced time for the Li-ion diffusion. The CNF/Sn electrode exhibits a poor rate capability, suggesting that the existing design of carbon and Sn nanocomposites was sufficient for the rapid ion diffusion at high rate current densities. Hence, the debossed structure of DCNF/Sn electrode has been designed to improve the diffusion way of Li ions. Interestingly, the DCNF/Sn electrode had the excellent rate capability of 687 mAh g^{-1} to 482 mAh g^{-1} at different current densities ranging from 100 mA g^{-1} to 2000 mA g^{-1} . Furthermore, the enhanced rate capability of DCNF/Sn electrode was the higher as compared with the previously reported electrodes using carbon and Sn nanocomposites (see Fig. 8b) [33–35,37–41]. Moreover, the cycling stability at high current density is essential for the use of LIBs in real-life applications. Fig. 8c presents the cycling stability at the high current density of 2000 mA g^{-1} for the CNF/Sn and DCNF/Sn electrodes over 500 cycles. The CNF/Sn electrode has a poor cycling stability with the discharge specific capacity of 31 mAh g^{-1} at 2000 mA g^{-1} .

The aggregation of Sn for the CNF/Sn electrode (see Fig. 9a and b) was observed after 500 cycles, suggesting that a low ionic diffusion performance could reduce the ultrafast cycling stability. At the same time, the DCNF/Sn electrode (Fig. 9c and d) displayed the outstanding ultrafast cycling stability with the discharge specific capacity of 275 mAh g^{-1} at 2000 mA g^{-1} after 500 cycles without any changes from the initial structure. The improved performance of DCNF/Sn electrode should be attributed to the improved ionic diffusion capability and the efficient transfer way for electrons based on the debossed structure.

Therefore, in this study, we confirmed that the enhanced energy storage performance at a high current density can be explained as shown in Fig. 10a. In our results, the introduction of carbon matrix for the Sn nanoparticles was able to efficiently deliver the excellent cycling stability with high discharge capacities from the effective accommodation of dramatic volume changes for the Sn nanoparticles during cycling. In addition, the novel debossed structure proposed in the present study also leads to a remarkably ultrafast cycling stability resulting from the improved ionic diffusion

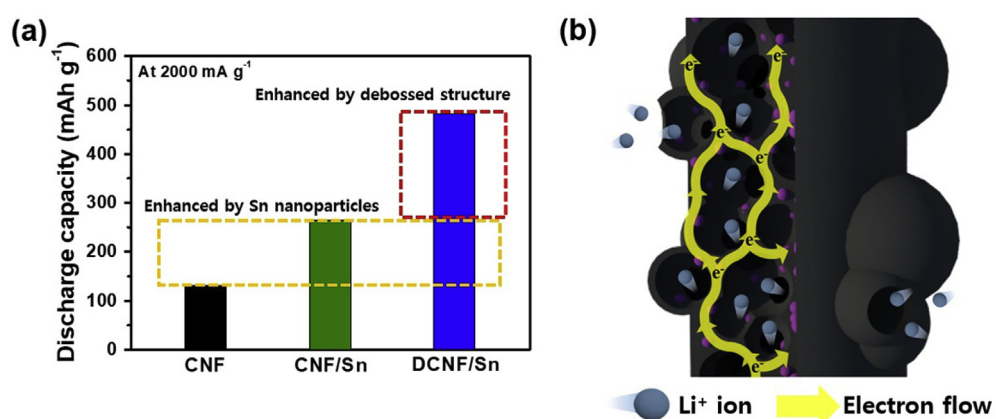


Fig. 10. (a) The discharge specific capacity of CNF, CNF/Sn, and DCNF/Sn electrodes showing the enhanced capacity due to the Sn nanoparticles and the debossed structure; (b) the proposed model of the DCNF/Sn electrode during cycling with the diffusion process of Li ions and the electron transfer.

performance for Li ions, as well as to an expeditious transfer way for electrons (see Fig. 10b).

3. Conclusions

In the present study, DCNF/Sn fabricated by electrospinning, carbonization and the debossing process exhibited a novel debossed structure with halls (40–90 nm). The resulting impressive energy storage performances of the DCNF/Sn electrode with excellent cycling stability and high discharge capacity (677 mA h g⁻¹ after 100 cycles at 100 mA g⁻¹), a noticeable rate capability (482 mA h g⁻¹ at 2000 mA g⁻¹), and a remarkable ultrafast cycling stability (275 mA h g⁻¹ after 500 cycles at 2000 mA g⁻¹) can clearly be attributed to the following two reasons: (i) the outstanding cycling stability with a high discharge capacity is obtained from the effective accommodation of dramatic volume changes for the Sn nanoparticles having a high capacity using the carbon matrix.; (ii) the remarkably ultrafast performance indicates that the debossed structure is due to the improvement of the ionic diffusion capability. Thus, the novel design of debossed structure is a new approach both realization of the ultrafast energy storage and an enhancement of the ionic diffusion capability for practical applications of LIBs.

Acknowledgments

This work was supported by the Technology Innovation Program (10080656, Development of ceramic/carbon convergence and integration anode material for 10C fast charging Lithium ion battery) funded By the Ministry of Trade, Industry & Energy (MOTIE, Korea).

Appendix A. Supplementary data

Supplementary data related to this article can be found at <https://doi.org/10.1016/j.jallcom.2018.06.072>.

References

- [1] M. Armand, J.-M. Tarascon, Building better batteries, *Nature* 451 (2008) 652–657.
- [2] P.G. Bruce, B. Scrosati, J.-M. Tarascon, Nanomaterials for rechargeable lithium batteries, *Angew. Chem. Int. Ed.* 47 (2008) 2930–2946.
- [3] G.-H. An, H.-J. Kim, H.-J. Ahn, Improved ionic diffusion through the mesoporous carbon skin on silicon nanoparticles embedded in carbon for ultrafast lithium storage, *ACS Appl. Mater. Interfaces* 10 (2018) 6235–6244.
- [4] J.W. Choi, D. Aurbach, Promise and reality of post-lithium-ion batteries with high energy densities, *Nat. Rev. Mater.* 1 (2016) 16013.
- [5] G.-H. An, D.-Y. Lee, H.-J. Ahn, Tunneled mesoporous carbon nanofibers with embedded ZnO nanoparticles for ultrafast lithium storage, *ACS Appl. Mater. Interfaces* 9 (2017) 12478–12485.
- [6] H. Ning, H. Xie, Q. Zhao, J. Liu, W. Tian, Y. Wang, M. Wu, Electrospinning ZnO/ carbon nanofiber as binder-free and self-supported anode for Li-ion batteries, *J. Alloys Compd.* 722 (2017) 716–720.
- [7] G.-H. An, D.-Y. Lee, H.-J. Ahn, Tofu-derived carbon framework with embedded ultrasmall tin nanocrystals for high-performance energy storage devices, *J. Alloys Compd.* 722 (2017) 60–68.
- [8] D. Wu, Q. Kuang, Y. Zhao, S. Liu, Q. Fan, Sol-gel synthesized carbon-coated vanadium borate as anode material for rechargeable Li and Na batteries, *J. Alloys Compd.* 732 (2018) 506–510.
- [9] G.-H. An, D.-Y. Lee, H.-J. Ahn, Ultrafast lithium storage using antimony-doped tin oxide nanoparticles sandwiched between carbon nanofibers and a carbon skin, *ACS Appl. Mater. Interfaces* 8 (2016) 30264–30270.
- [10] M. Qi, Y. Zhong, M. Chen, Y. Dai, X. Xia, Hollow nickel microtube/carbon nanospheres Core-Shell arrays as electrode material for rechargeable Li-ion batteries, *J. Alloys Compd.* 750 (2018) 715–720.
- [11] Y. Teng, M. Mo, Y. Li, J. Xue, H. Zhao, Amorphous carbon-coated ZnO porous nanosheets: facile fabrication and application in lithium- and sodium-ion batteries, *J. Alloys Compd.* 744 (2018) 712–720.
- [12] G.-H. An, H.-J. Ahn, Ultrafast lithium storage of high dispersed silicon and titanium oxide nanoparticles in carbon, *J. Alloys Compd.* 710 (2017) 274–280.
- [13] C. Zhu, C.-G. Han, G. Saito, T. Akiyama, Facile synthesis of MnO/carbon composites by a single-step nitrate-cellulose combustion synthesis for Li ion battery anode, *J. Alloys Compd.* 689 (2016) 931–937.
- [14] G.-H. An, H.-J. Ahn, Carbon nanofiber/cobalt oxide nanop pyramid core-shell nanowires for high-performance lithium-ion batteries, *J. Power Sources* 272 (2014) 828–836.
- [15] J.Y. Lee, T.J. Hwang, J.S. Oh, J.M. Kim, Y.M. Jeon, Y. Piao, Sn/SnO_x -loaded uniform-sized hollow carbon spheres on graphene nanosheets as an anode for lithium-ion batteries, *J. Alloys Compd.* 736 (2018) 42–50.
- [16] S. Gao, A.-M. Wu, X.-Z. Jin, F. Ye, X.-L. Dong, J.-Y. Yu, H. Huang, Nanostructured Sn-M (M = Cu, Mg and Fe) intermetallic alloys and their electrochemical activity as anode electrodes in a Li-ion battery, *J. Alloys Compd.* 706 (2017) 401–408.
- [17] S. Sengupta, A. Patra, M. Akhtar, K. Das, S.B. Majumder, S. Das, 3D microporous Sn-Sb-Ni alloy impregnated Ni foam as high-performance negative electrode for lithium-ion batteries, *J. Alloys Compd.* 705 (2017) 290–300.
- [18] P. Dou, Z. Cao, J. Zheng, C. Wang, X. Xu, Solid polymer electrolyte coating three-dimensional Sn/Ni bimetallic nanotube arrays for high performance lithium-ion battery anodes, *J. Alloys Compd.* 685 (2016) 690–698.
- [19] H.Y. Yue, Z. Shi, L. Wang, X. Li, H.Y. Dong, Y.H. Yin, S. Yang, Rapid calcination synthesis of Zn₂SnO₄@C/Sn composites for high- performance lithium ion battery anodes, *J. Alloys Compd.* 723 (2017) 1018–1025.
- [20] R. Liu, W. Su, P. He, C. Shen, C. Zhang, F. Su, C.-A. Wang, Synthesis of SnO₂/Sn hybrid hollow spheres as high performance anode materials for lithium ion battery, *J. Alloys Compd.* 688 (2016) 908–913.
- [21] Y. Liang, Z.G. Tian, H.J. Liu, R. Peng, Synthesis and characterization of Sn–Mo mixtures as negative electrode materials for Li-ion batteries, *J. Alloys Compd.* 504 (2010) 50–52.
- [22] Y.-G. Huang, Q.-C. Pan, H.-Q. Wang, Z.-X. Yan, G.-H. Yang, Y.H. Chen, Q. Wu, Q.-Y. Li, Sn/SnO_x embedded in carbon nanosheets as high-performance anode material for lithium ion battery, *Ceram. Int.* 42 (2016) 4586–4593.
- [23] Q.-C. Pan, Y.-G. Huang, H.-Q. Wang, G.-H. Yang, L.-C. Wang, J. Chen, Y. Zan, Q.-Y. Li, MoS₂/C nanosheets Encapsulated Sn@SnO_x nanoparticles as high-performance Lithium-ion battery anode material, *Electrochim. Acta* 197 (2016) 50–57.
- [24] G.-H. An, D.-Y. Lee, H.-J. Ahn, Vanadium nitride networks with encapsulated carbon fibre furrowed porous surfaces for ultrafast asymmetric supercapacitors with robust cycle life, *J. Mater. Chem. A* 5 (2017) 19714–19720.
- [25] G.-H. An, D.-Y. Lee, H.-J. Ahn, Carbon-Encapsulated hollow porous vanadium-oxide nanofibers for improved lithium storage properties, *ACS Appl. Mater. Interfaces* 8 (2016) 19466–19474.
- [26] G.-H. An, H.-J. Ahn, Carbon- Activated porous carbon nanofibers using Sn segregation for high-performance electrochemical capacitors, *Carbon* 65 (2013) 87–96.
- [27] Y.-W. Lee, D.-M. Kim, S.-J. Kim, M.-C. Kim, H.-S. Choe, K.-H. Lee, J.I. Sohn, S.N. Cha, J.M. Kim, K.-W. Park, In situ synthesis and characterization of Ge embedded electrospun carbon nanostructures as high performance anode material for lithium-ion batteries, *ACS Appl. Mater. Interfaces* 8 (2016) 7022–7029.
- [28] D. Deng, J.Y. Lee, Reversible storage of lithium in a rambutan-like tin–carbon electrode, *Angew. Chem. Int. Ed.* 48 (2009) 1660–1663.
- [29] M. Alaf, D. Gultekin, H. Akbulut, Electrochemical properties of free-standing Sn/SnO_x/multi-walled carbon nanotube anode papers for Li-ion batteries, *Appl. Surf. Sci.* 275 (2013) 244–251.
- [30] J. Zhang, Z. Ma, W. Jiang, Y. Zou, Y. Wang, C. Lu, Sandwich-like CNTs@SnO_x/SnO_x anodes on three-dimensional Ni foam substrate for lithium ion batteries, *J. Electroanal. Chem.* 767 (2016) 49–55.
- [31] K.-C. Hsu, C.-E. Liu, P.-C. Chen, C.-Y. Lee, H.-T. Chiu, One-step vapor–solid reaction growth of Sn@C core–shell nanowires as an anode material for Li-ion batteries, *J. Mater. Chem. B* 22 (2012) 21533–21539.
- [32] G. Wang, Y.Q. Ma, Z.Y. Liu, J.N. Wu, Novel highly porous Sn–C composite as high performance anode material for lithium-ion batteries, *Electrochim. Acta* 65 (2012) 275–279.
- [33] C. Cui, X. Liu, N. Wu, Y. Sun, Facile synthesis of core/shell-structured Sn/onion-like carbon nanocapsules as high-performance anode material for lithium-ion batteries, *Mater. Lett.* 143 (2015) 35–37.
- [34] Y. Hu, Q.-R. Yang, J. Ma, S.-L. Chou, M. Zhu, Y. Li, Sn/SnO_x@C composite nanofibers as advanced anode for lithium-ion batteries, *Electrochim. Acta* 186 (2015) 271–276.
- [35] B. Luo, B. Wang, M. Liang, J. Ning, X. Li, L. Zhi, Reduced graphene oxide-mediated growth of uniform tin-core/carbon-sheath coaxial nanocables with enhanced lithium ion storage properties, *Adv. Mater.* 24 (2012) 1405–1409.
- [36] Z. Li, W. Lv, C. Zhang, J. Qin, W. Wei, J.-J. Shao, D.-W. Wang, B. Li, F. Kang, Q.-H. Yang, Nanospace-confined formation of flattened Sn sheets in pre-seeded graphenes for Lithium ion batteries, *Nanoscale* 6 (2014) 9554–9558.
- [37] Q. Tian, Z. Zhang, L. Yang, S.-I. Hirano, Synthesis of Sn₂ dispersed in the Sn@carbon nanospheres interspaces of a three-dimensional SnO₂/Sn@carbon nanowires network, and their application as an anode material for lithium-ion batteries, *J. Mater. Chem. A* 2 (2014) 12881–12887.
- [38] Y. Yu, L. Gu, C. Wang, A. Dhanabalan, P.A.V. Aken, J. Maier, Encapsulation of Sn@carbon nanoparticles in bamboo-like hollow carbon nanofibers as an anode material in lithium-based batteries, *Angew. Chem. Int. Ed.* 48 (2009) 6485–6489.
- [39] P. Lian, J. Wang, D. Cai, G. Liu, Y. Wang, H. Wang, Design and synthesis of porous nano-sized Sn@C/graphene electrode material with 3D carbon network for high-performance lithium-ion batteries, *J. Alloys Compd.* 604

- (2014) 188–195.
- [40] X. Bai, B. Wang, H. Wang, J. Jiang, Preparation and electrochemical properties of profiled carbon fiber-supported Sn anodes for lithium-ion batteries, *J. Alloys Compd.* 628 (2015) 407–412.
- [41] L. Ji, Z. Tan, T. Kuykendall, E.J. An, Y. Fu, V. Battaglia, Y. Zhang, Multilayer nano assembly of Sn-nanopillar arrays sandwiched between graphene layers for high-capacity lithium storage, *Energy Environ. Sci.* 4 (2011) 3611–3616.